

Chasing the observational signatures of seed black holes at $z > 7$: candidate observability

Rosa Valiante¹ *, Raffaella Schneider^{1,2}, Luca Zappacosta¹, Luca Graziani¹,
Edwige Pezzulli^{1,2,3} and Marta Volonteri⁴

¹ *INAF-Osservatorio Astronomico di Roma, via di Frascati 33, 00078, Monteporzio Catone, Italy*

² *Dipartimento di Fisica, Università di Roma “La Sapienza”, P.le Aldo Moro 2, 00185, Roma, Italy*

³ *INFN, Sezione di Roma I, P.le Aldo Moro 2, I-00185 Roma, Italy*

⁴ *CNRS, UMR 7095, Institut d’Astrophysique de Paris, F-75014, Paris, France*

Accepted . Received

ABSTRACT

Observing the light emitted by the first accreting black holes (BHs) would dramatically improve our understanding of the formation of quasars at $z > 6$, possibly unveiling the nature of their supermassive black hole (SMBH) seeds. In previous works we explored the relative role of the two main competing BH seed formation channels, Population III remnants (low-mass seeds) and direct collapse BHs (high-mass seeds), investigating the properties of their host galaxies in a cosmological context. Building on this analysis, we predict here the spectral energy distribution and observational features of low- and high-mass BH seeds selected among the progenitors of a $z \sim 6$ SMBH. We derive the processed emission from both accreting BHs and stars by using the photo-ionization code Cloudy, accounting for the evolution of metallicity and dust-to-gas mass ratio in the interstellar medium of the host galaxies, as predicted by the cosmological data-constrained model GAMETE/QSODUST. We show how future missions like JWST and ATHENA will be able to detect the light coming from SMBH progenitors already at $z \sim 16$. We build upon previous complementary studies and propose a method based on the combined analysis of near infrared (NIR) colors, IR excess (IRX) and UV continuum slopes (i.e. color-color and IRX- β diagrams) to distinguish growing seed BH host galaxies from starburst-dominated systems in JWST surveys. Sources selected through this criterion would be the best target for follow-up X-ray observations.

Key words: Galaxies: evolution, high-redshift, nuclei; quasars: general, supermassive black holes;

1 INTRODUCTION

Recent theories of BH formation predict at least two viable mechanisms explaining the formation of accreting SMBHs of $10^9 - 10^{10} M_{\odot}$, which are observed already at redshift $z \sim 7$: the rapid growth of Population III (Pop III) remnant BHs ($\sim 100 M_{\odot}$) (e.g. Madau & Rees 2001; Heger et al. 2003; Yoshida et al. 2008; Latif et al. 2013; Hirano et al. 2015), driven by the accretion of gas at rates exceeding the Eddington limit or the formation of more massive BH seeds, the so-called direct collapse BHs (DCBHs), of $(10^5 - 10^6) M_{\odot}$ (e.g. Bromm & Loeb 2003; Lodato & Natarajan 2006, 2007; Begelman et al. 2006; Volonteri et al. 2008; Inayoshi & Omukai 2012; Ferrara et al. 2014; Agarwal et al. 2014; Inayoshi et al. 2015). We refer the readers to a number of ded-

icated reviews for more details on different seed formation and growth mechanisms (Volonteri 2010; Natarajan 2011; Latif & Ferrara 2016; Johnson & Haardt 2016; Gallerani et al. 2017; Valiante et al. 2017b, and references therein).

Several semi-analytic models have been devoted to study the formation of SMBHs, exploring the role of low-mass or high-mass seeds (e.g. Volonteri et al. 2003; Volonteri & Rees 2005, 2006; Madau et al. 2004; Haiman 2004; Tanaka & Haiman 2009; Volonteri et al. 2015, and references therein). Petri et al. (2012) presented the first semi-analytic model for the formation of high redshift SMBHs exploring the combined action of low- ($100 M_{\odot}$) and high-mass ($10^5 M_{\odot}$) seed BHs. In all those works, however, seeds were not planted according to the environmental conditions and the chemical evolution of the interstellar medium (ISM) of the host galaxies was not considered.

In a previous work (Valiante et al. 2016, hereafter

* E-mail: rosa.valiante@oa-roma.inaf.it

V16), we used a cosmological, data-constrained model, GAMETE/QSO_{DUST} to investigate the relative role of low-mass (light) and high-mass (heavy) BH seed in the formation of $z > 6$ SMBHs, like the one powering the quasar SDSS J1148+5251. GAMETE/QSO_{DUST} consistently follows the formation and evolution of nuclear BHs and their host galaxies along different merger histories of the parent DM halo. While many semi-analytical models and simulations follow BH growth, star formation and metals, GAMETE/QSO_{DUST} is the only model that traces accurately dust evolution as well.

In V16 we showed that in a Eddington-limited BH accretion scenario, despite their low occurrence (in just few halos, 3-30 depending on the merger history), the formation of DCBHs is required to grow a SMBH with $M_{\text{BH}} > 10^9 M_{\odot}$. Moreover, in Pezzulli et al. (2016) we showed that a mildly super-critical growth (less than 20 times the Eddington rate) onto light BH seeds of $100 M_{\odot}$ is required to reproduce the mass of SDSS J1148+5251 if heavy seeds are not considered in our model.

Despite intensive efforts, no observational signatures of high redshift SMBHs progenitors have been found in current surveys (see e.g. Reines & Comastri 2016, for a recent review). To date, no clear AGN signatures at $z > 6$ have been found even in the deepest X-ray observations (Willott 2011; Treister et al. 2013; Weigel et al. 2015; Vito et al. 2016; Cappelluti et al. 2016; Luo et al. 2017). It should be noted though, that two faint AGN candidates, with photometric redshift $z = 6.6$ and $z = 9.7$, have been selected in the CANDELS GOODS-S field (Giallongo et al. 2015). Although the redshift determination is still uncertain (Georgakakis et al. 2015; Cappelluti et al. 2016; Luo et al. 2017), these sources have been proposed as possible DCBH hosts by Pacucci et al. (2016).

A clear example of the difficulties in interpreting observations at high redshift is the controversial nature of the metal poor component of the bright Ly α emitter CR7 observed by Matthee et al. (2015), Sobral et al. (2015), and Bowler et al. (2016) at redshift $z \sim 6.6$. This is suggested to be either a DCBH (Pallottini et al. 2015; Hartwig et al. 2015; Agarwal et al. 2016; Smith et al. 2016; Smidt et al. 2016; Agarwal et al. 2017; Pacucci et al. 2017) or a Pop III stars host candidate (Sobral et al. 2015; Visbal et al. 2016; Dijkstra et al. 2016), or none of the two Bowler et al. (2016).

If faint AGNs at high redshift are powered by accreting DCBHs, the non detection of AGN candidates in current surveys may be explained by the peculiar and rare environmental conditions required for DCBHs formation (Hosokawa et al. 2012; 2013; Inayoshi et al. 2014; Inayoshi & Haiman 2014; Yue et al. 2014; Dijkstra et al. 2014; Sugimura et al. 2015; Habouzit et al. 2016; Chon et al. 2016; Valiante et al. 2016). On the other hand, the current lack of detection in the X-ray band could be due to short and intermittent super-Eddington accretion events on Pop III remnants, resulting in a very low active BH fraction ($\sim 1\%$) at $z > 7$ (Pezzulli et al. 2017).

Theoretical models of the expected spectral energy distribution (SED) of AGNs at $z > 4-5$ may provide a powerful tool to support future observations. Indeed, with the upcoming *James Webb Space Telescope* JWST and *Advanced Telescope for High Energy Astrophysics* (ATHENA, in the next decade) missions we may be able to detect the signa-

tures of active galaxies up to very high redshifts. Pacucci et al. (2015) modeled the SED of a growing DCBH with initial mass of $10^5 M_{\odot}$ accreting gas in a metal-free isolated DM host halo. They use the code Cloudy (Ferland et al. 2013) to process the intrinsic (optical/UV/X-ray) emission, suggesting that the resulting infrared (IR) emission around $\sim 1 \mu\text{m}$ and the $[0.1 - 10]$ keV band X-ray emission may be detected by JWST and ATHENA. Subsequently, Natarajan et al. (2017) extended this study to what they call *obese black hole galaxies* (OBGs), a class of transient objects predicted by Agarwal et al. (2013) that originate from the merging of star forming galaxies with a neighbor satellite DCBH host. The authors presented a color-color selection criteria aimed at identifying OBGs with predicted magnitudes $M_{\text{AB}} < 25$, that should be detected by the JWST instrument MIRI. They compared the SEDs of OBGs and of growing Pop III remnant BHs at redshift $z = 9$, concluding that JWST could be able to discriminate among the two seed formation channels. In addition, Volonteri et al. (2017) presented a population synthesis model for high redshift BHs, AGN and galaxies, based on empirical relations, proposing a color-color selection in JWST photometric bands, F1280W-F2100W vs F200W-F1280W, to discriminate starburst dominated galaxies and AGN in future surveys.

The studies mentioned above introduced promising methods to search for AGN and seed BHs candidates in future surveys, setting the (theoretical) groundwork for the upcoming high redshift multi-wavelength observations. However, the systems analyzed in Natarajan et al. (2017) and Volonteri et al. (2017) are not explicitly related to the formation of a SMBH with the mass and accretion rate sufficient to explain the luminous quasars at $z \sim 6$ and do not grow in its environment.

In Valiante et al. (2017a, hereafter paperI) we presented a statistical analysis of the properties of “isolated” galaxies that host light (low-mass) or heavy (high-mass) BH seeds¹. We named these systems (BH + host galaxy) *isolated light seeds* (ILS) and *isolated heavy seeds* (IHS). Following V16, ILS and IHS have been selected among the progenitors of SDSS J1148+5251. In paperI we pointed out that at $z > 10$ the majority of heavy ($\sim 98\%$) and light (80%) seeds evolve in isolation and that these two populations show different properties: IHS have BH accretion rate higher than ILS; IHS host galaxies show a factor of 5-10 lower stellar mass and metallicity as well as a less efficient star formation history. These differences become statistically negligible at $z \leq 10$, when the fraction of IHS (ILS) drops to less than ~ 2 (20)% as a consequence of merger events. At these later epochs, any trace of the BH seed origin and of its birth environment is lost. Thus, candidate systems at $z > 10$ are the best targets to discriminate among the two main seed formation channels.

Here we compute the SED of IHS and ILS, using the sample presented in paperI. Our aim is to establish the feasibility of: (i) detecting high- z faint progenitors of the first SMBHs, (ii) observationally discriminating light and heavy BH seeds. Similarly to Pacucci et al. (2015) and Natarajan et al. (2017), we use Cloudy to model the SEDs of IHS and

¹ Starting from the epoch of the BH seed formation, we consider a system (BH and its host galaxy) to evolve in “isolation” until a minor or major galaxy merger takes place.

ILS. The main difference of our approach is that we analyze systems (BHs-host galaxies) selected among the ancestors population of an observed SMBH, along its cosmological evolution. In other words, our approach has the advantage of following the evolution of light and heavy seed progenitors along the same hierarchical history (i.e. the two seed BHs formation channels are not mutually exclusive), starting from the epoch at which the first stars form ($z \sim 24$), down to $z \sim 6$, when the observed quasar is eventually assembled. The properties of the seed BH population are closely related to the evolution of their host galaxies: mass, number, redshift distribution and growth history are regulated by the build up of the UV radiation field, by the metals and dust pollution of the ISM and intergalactic medium (IGM) and by the effect of stellar and AGN-driven winds. Our approach allows to assess the possibility of observationally distinguishing the two different populations of seed BHs.

The paper is organized as follows. In Section 2 we present the model for the SEDs. In Section 3 we discuss in details two accreting heavy and two accreting light seed BH prototypes, inspecting their predicted SEDs. Finally, we discuss our results drawing the conclusions of the study in Sections 4 and 5.

2 SUMMARY OF THE MODEL

Here we summarize the main features of GAMETE/QSODUST, a semi-analytic, data-constrained model developed to study the formation and evolution of high-redshift quasars and their host galaxies in a cosmological framework. We refer the reader to Valiante et al. (2011, 2014, 2016, and paper I, for further details on GAMETE/QSODUST)².

GAMETE/QSODUST successfully reproduced the observed properties of a sample of quasars at $z > 5$ (Valiante et al. 2014). Following V16, we focus our analysis on the progenitor BHs of the $(2 - 6) \times 10^9 M_\odot$ SMBH which powers SDSS J1148+5251, one of the best studied luminous quasars at $z > 6$. A summary of the properties of SDSS J1148+5251 inferred from the observations can be found in Valiante et al. (2011, 2014).

Dark matter halo merger trees. Different hierarchical merger histories (merger trees) of the $10^{13} M_\odot$ host dark matter (DM) halo have been reconstructed by using a Monte Carlo algorithm following the Extended Press-Schechter theory. The DM halo resolution mass at $z > 14$ is extended to halos with virial temperature in the range $1200 \text{ K} \leq T_{\text{vir}} < 10^4 \text{ K}$ (i.e. mini-halos). These mini-halos dominate the halo mass spectrum at $z \gtrsim 17$ and are expected to host the first generation of stars (Pop III stars). At $z > 14$ instead the merger tree halo population is dominated by Ly α halos, namely DM halos with $T_{\text{vir}} \geq 10^4 \text{ K}$ (see V16 for details).

BH growth. The growth of the BH is driven by gas accretion and mergers. The BH accretion rate is described by the Bondi-Hoyle-Lyttleton formula re-scaled by a factor $\alpha_{\text{BH}} = 50$ (to match the BH mass of SDSS J1148+5251)³ and can not exceed the Eddington limit (see Valiante et al. 2014, for details).

Star formation and ISM chemical evolution. In each progenitor galaxy, stars are assumed to form following a series of quiescent and/or major merger-enhanced bursts⁴. Following each star formation episode, the production of metals and dust by Asymptotic Giant Branch (AGB) stars and Supernovae (SNe) is regulated by the stellar lifetimes. In addition, we include physical prescriptions for dust processing in a two-phase ISM: destruction by SN shocks in the hot, diffuse medium and grain growth in cold, dense molecular clouds (see Valiante et al. 2014; de Bennassuti et al. 2014, for details).

Mechanical feedback. We also include energy-driven winds, triggered by SNe and accreting BHs. The metal and dust rich gas outflows, launched on galaxy-scales, are responsible for polluting the IGM. This mechanical feedback is described assuming that 0.2 (0.25)% of the energy released by SN explosions (BH accretion) is used to accelerate the ISM gas (see Valiante et al. 2012, and V16 for details). As observed in SDSS J1148+5251 (Maiolino et al. 2012; Ciccone et al. 2015), in our model the evolution history of BHs and their host galaxies is mainly regulated by AGN feedback, with SN-driven winds having only a minor effect.

2.1 First stars and BH seeds formation

As discussed in V16, the number and nature of stars and BH seeds is determined by the combined effect of chemical and radiative feedback.

The level of chemical enrichment determines the duration of the Pop III star formation era. Pop III stars form out of metal poor gas when the ISM metallicity is lower than the adopted critical threshold $Z_{\text{cr}} \sim 10^{-4} Z_\odot$ (Schneider et al. 2002, 2003, 2012). The Pop III initial mass function (IMF) is assumed to be a Larson IMF (Larson 1998) with a characteristic mass $m_{\text{ch}} = 20 M_\odot$ (top-heavy IMF), whereas for Pop II we adopt $m_{\text{ch}} = 0.35 M_\odot$ (standard IMF).

In addition, the level of intensity of H₂ photo-dissociating radiation, to which halos are exposed, determines whether stars (in mini-halos) or DCBHs (in Ly α cooling halos) form and regulates the star formation efficiency in mini-halos (according to the halo virial temperature, redshift and metallicity, see Appendix A in V16 and de Bennassuti et al. 2017).

When the star formation efficiency is low, we perform a stochastic sampling of the intrinsic Pop III top-heavy IMF, randomly selecting stars in the mass range $[10 - 300] M_\odot$ until the total stellar mass formed in the burst is reached. Light

² The model GAMETE (GALaxy MERger Tree and Evolution) was originally conceived to study the formation and evolution of local, Milky-Way like galaxies, in a cosmological context (Salvadori et al. 2007, 2008)

³ α_{BH} is a free parameter required in semi-analytic models and numerical simulations to account for the higher central densities around accreting BHs (e.g. Di Matteo et al. 2005).

⁴ A major merger is defined as the coalescence of two DM halos with mass ratio (less massive over the most massive) $\mu > 1/4$

BH seeds are formed by the collapse of Pop III stars with masses in the range $[40 - 140] M_{\odot}$ and $[260 - 300] M_{\odot}$ ⁵.

In Ly α -cooling halos, heavy BH seeds ($10^5 M_{\odot}$) can form when $Z < Z_{\text{cr}}$ and the cumulative Lyman Werner (LW) emission (from all galaxies and AGN) is larger than the assumed critical value $J_{\text{cr}} = 300 \times 10^{-21}$ erg/s/Hz/cm²/sr (see Valiante et al. 2017b, and references therein, for a discussion regarding J_{crit}). As shown in V16, the critical level is reached at $z \sim 16 - 18$, depending on the particular merger history.

We stop forming Pop III stars and BH seeds at $z < 15$, when metal enrichment to $Z > Z_{\text{cr}}$ triggers the transition to Pop II star formation.

3 SPECTRAL ENERGY DISTRIBUTION MODELS

In this section, we describe how we derive the SED of galaxies hosting the first seed BHs. Once GAMETE/QSODUST has predicted the physical quantities for each galaxy and its central BH (i.e. the time-dependent BH mass, BH accretion rate, gas density, star formation rate, stellar mass, ISM metallicity and dust-to-gas ratio), we compute the expected intrinsic emission of the central accreting BH and stellar component, separately. Then, we process the combined emission by means of the plasma photo-ionization code Cloudy, which models the physical conditions of clouds (ionization, chemical and thermal state) exposed to emitting sources. Calculations were performed with version 13.04 of Cloudy⁶ (Ferland et al. 2013).

3.1 Stellar component

The intrinsic emission from Pop III stars is computed as the sum of single stellar Black Body (BB) spectra, depending on the randomly extracted stellar masses. We compute the BB by using the stellar effective temperatures given by Schaerer (2002).

The SED of Pop II stars are computed with the spectral evolution code PEGASE v2.0⁷ (Fioc & Rocca-Volmerange 1997; 1999). As an input to the code, we provide the Larson IMF (not included in the original version) and the file containing the star formation and metallicity evolution histories (as a function of time, for each progenitor galaxy) as predicted by GAMETE/QSODUST.

3.2 Accreting BHs

The intrinsic SED of accreting BHs has been modelled as described in Pezzulli et al. (2017). The optical/UV primary emission from the accretion disc is the sum of multicolor Black Body (BB) spectra given by:

$$L_{\nu}^{\text{BB}} \propto \int_0^{T_{\text{max}}} B_{\nu}(T) \left(\frac{T}{T_{\text{max}}} \right)^{-11/3} \frac{dT}{T_{\text{max}}}, \quad (1)$$

where $B_{\nu}(T)$ is the Planck function and T the disc temperature, which reaches the maximum value, T_{max} , nearby the innermost stable circular orbit (ISCO). $T(r)$ is the temperature profile of steady-state, optically thick, geometrically thin accretion disc described by Shakura & Sunyaev (1973, see Pezzulli et al. 2017 for further details). The template spectrum is normalized to the accreting BH bolometric luminosity.

The part of the spectrum in the X-ray energy band due to the emission from the hot corona is modeled with a power law with an exponential cut-off at energy $E_c = 300$ keV (Sazonov et al. 2004; Yue et al. 2013): $L_{\nu} \propto \nu^{-\Gamma+1} e^{-h\nu/E_c}$. We include the contribution of the metallicity-dependent reflection component (the primary X-ray emission reflected by the surrounding neutral medium) using the reflection-only solution of the PEXRAV model (Magdziarz & Zdziarski 1995) in the XSPEC code⁸.

Following Brightman et al. (2013), we consistently compute the photon index, Γ , in the hard X-ray band (2 – 10 keV) for each accreting BH as a function of the Eddington ratio λ_{Edd} (predicted by GAMETE/QSODUST) as: $\Gamma_{2-10\text{keV}} = 0.32 \log \lambda_{\text{Edd}} + 2.27$.

3.3 Emerging spectrum

The AGN and stellar intrinsic emission components are used as an input to Cloudy. The emerging SED is the result of the total intrinsic radiation reprocessed by the column of gas, enriched by atomic metals and dust, present in the host galaxy.

We assume a static, spherical geometry for the material distribution within the galaxy. In Cloudy, the spherical gas cloud configuration is described by distributing the material in concentric shells with progressively larger radii. The inner shell face is illuminated by the radiation coming from a combination of point-like sources placed at the center.

To compute the emerging spectrum, Cloudy requires the following set of parameters:

- inner and outer radii of the sphere, r_{in} and r_{out} ;
- gas number density at the inner radius $n(r_{\text{in}})$ and the power index, α , of the gas radial density profile;
- gas composition: column of hydrogen, helium, atomic metals (or gas metallicity) and dust-to-gas ratio.

In GAMETE/QSODUST, the gas density profile is described by a singular isothermal sphere with a flat core:

$$n(r) = \frac{n_{\text{norm}}}{1 + (r/r_{\text{core}})^2}. \quad (2)$$

The term n_{norm} is the normalization constant set by the condition that the total gas mass of the galaxy is enclosed within the halo virial radius, R_{vir} . A core radius of $r_{\text{core}} = 0.1$ (0.01) pc has been chosen to encompass the small scale of the inner, higher-density regions around the central accreting heavy (light) seed BH⁹.

⁵ We assume that only the most massive BH among the Pop III remnants formed in each burst settles in the center of the halo accreting gas from its surrounding.

⁶ www.nublado.org

⁷ http://www2.iap.fr/users/fioc/PEGASE.html

⁸ We consistently linked Γ , E_c and normalization parameter to the values adopted for the primary powerlaw component and set the inclination angle to 60° and the reflection strength parameter, $R = 1$, consistent with typical values of local low-luminosity AGN (Burlon et al. 2011, Zappacosta et al. 2017; Del Moro et al. 2017)

⁹ As a comparison, the radius of gravitational influence of a BH, \sim

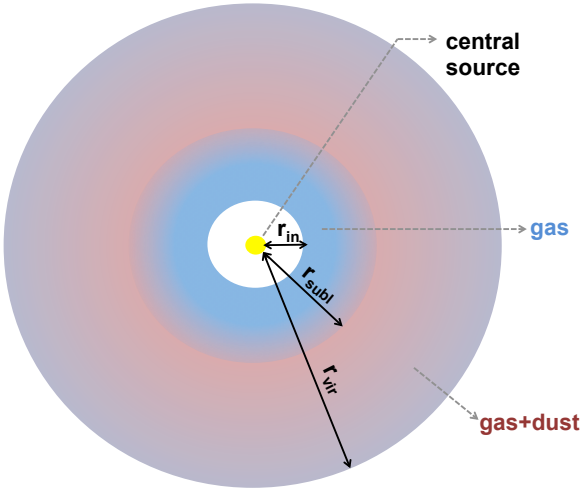


Figure 1. Schematic view of the geometry adopted for Cloudy simulations (see text for details). Different black solid arrows show the inner, r_{in} , sublimation, r_{subl} , and DM halo virial radius, r_{vir} . Dust free gas is distributed in the inner $r < r_{\text{subl}}$ shell, while the dusty ISM of the host extends from r_{subl} to r_{vir} .

We adopt the inner radius $r_{\text{in}} = r_{\text{core}}$ and the number density $n(r_{\text{in}}) = n_{\text{norm}}$ as input values for the Cloudy simulations and select the Cloudy density profile $n(r) = n(r_{\text{in}})(r/r_{\text{in}})^{\alpha} \text{cm}^{-3}$ with $\alpha = 2$, that closely match the profile of eq. 2 adopted in the GAMETE/QSODUST calculation. The outer radius is set to be $r_{\text{out}} = R_{\text{vir}}$. A schematic representation of the adopted geometry is given in Fig. 1.

The host galaxy metallicity and dust-to-gas ratio predicted by GAMETE/QSODUST are transferred to the Cloudy computation by rescaling the built-in table “ISM” abundances which accounts for metals and dust mixtures¹⁰.

We have verified that dust grains in the very inner regions (i.e. in the shells closer to the emitting source) can be heated above the sublimation limit. In other words, the maximum temperature of a grain species exceeds the default sublimation temperature (1400 K and 1750 K for silicate and graphite grains, respectively). Ignoring this aspect may overestimate the IR emission. To account for dust sublimation, when required, we perform simulations with Cloudy adopting the following three-step strategy (runs):

- (i) We determine the dust sublimation radius, r_{subl} (with $r_{\text{subl}} > r_{\text{in}}$), at which the temperature of the hottest grain species first falls below the sublimation temperature (run 1);
- (ii) We process the accreting BH emission traveling through the inner dust-free shell of depth $r_{\text{subl}} - r_{\text{in}}$. Thus, the inner shell of the cloud is heated only by the AGN (run 2);
- (iii) We combine the transmitted BH emission, resulting from run 2, with the emission from stellar sources and give

GM_{BH}/c_s^2 is ~ 3 pc for $M_{\text{BH}} = 10^5 M_{\odot}$ ($c_s \sim 15$ km/s for $T_{\text{gas}} = 10^4$ K) and ~ 0.03 pc for $M_{\text{BH}} = 100 M_{\odot}$ ($c_s \sim 5$ km/s for $T_{\text{gas}} = 10^3$ K).

¹⁰ In Cloudy the “ISM” gas-phase abundances are from Cowie & Songaila (1986), Savage & Sembach (1996), Snow et al. (2007), and Mullan et al. (1998) and the dust grain model is from Mathis et al. (1977).

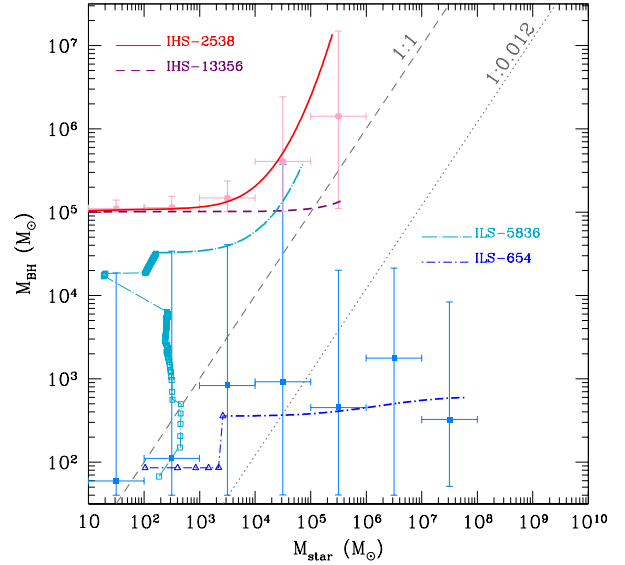


Figure 2. The BH mass as a function of the stellar mass for the selected accreting seed BHs prototypes. Solid and dashed lines are IHS-2538 and 13356, respectively. Two ILS are instead shown with dot-dashed (654) and dot-long-dashed (5836) curves. For these systems, data points indicated by squares (triangles) indicate the evolution during the Pop III star formation regime. We also label the fraction of systems in the IHS and ILS populations showing properties similar to each prototype (see text for details). Filled light blue squares and pink circles represent, respectively, the average BH mass of ILS and IHS in different stellar mass bins, with bars indicating the maximum and minimum BH mass in each bin and the width of the stellar mass interval. The dotted and short-dashed lines indicate the 1:1 and local BH-stellar mass (Sani et al. 2011) scaling relations.

the resulting SED as an input for a third Cloudy simulation for the outer shells, $r_{\text{subl}} \leq r \leq r_{\text{out}}$ (run 3).

This three-steps simulation strategy allows us to approximately mimic the fact that the AGN and stellar emission do not come from the same location in the host galaxy and are expected to be reprocessed by different gas and dust column densities. It is reasonable to assume that star forming regions are located on scales of few up to few hundreds pc (e.g. Davies et al. 2006, 2007; Wada et al. 2009; Hicks et al. 2009; Sani et al. 2012) where dusty molecular clouds can survive the destructive effects of the strong radiation field of the central AGN (i.e. in overdense regions where the cold, molecular gas is shielded by dust).

Finally, we include the redshift-dependent Cosmic Microwave Background radiation field, modeled by Cloudy as a BB spectrum with temperature $T_{\text{CMB}} = T_0(1+z)$ K (Peebles 1971; Mather et al. 1999; Wilkinson 1987).

4 RESULTS

In this section, we compute the time-dependent SED of four proto-typical ILS and IHS along their evolution. Since our main aim is to investigate if the nature of BH seeds can

be observationally discriminated, we select two efficiently-growing and two inefficiently-growing BH seeds among the IHS and ILS samples. In this way, we highlight differences in the same population of systems and similarities among the two different classes. In what follows, we indicate each system by its host halo ID assigned in the simulation merger tree.

4.1 Most and least massive BH in the sample

We have selected the most and least massive BH, in the sample analyzed in paperI. The physical and observational properties of these systems are representative of sources that we expect to find in biased regions that lead to the formation of a SMBH at $z > 6$.

Fig. 2 shows the evolution of selected ILS and IHS systems in the BH-stellar mass plane. The differences among the four tracks are indicative of the large variety of evolutionary channels that we find in the simulation.

The two IHS (2538 and 13356) are shown by the solid and dashed lines. Initially, they follow a similar evolution at constant BH mass. When the stellar mass of the hosts has reached a value of $10^3 M_\odot$, the BH mass of 2538 grows faster than the stellar mass, reaching a value of $\sim 10^7 M_\odot$, whereas 13356 continues to evolve at an almost constant BH mass. It is interesting to compare the evolution of these two systems with the average evolution of IHS, shown by the pink circles data points. It shows that 2538 better represents the average evolution of IHS hosted in galaxies with $M_{\text{star}} \leq 10^{4.5} M_\odot$. The fraction of systems similar to IHS-2538 ($\sim 33\%$) and 13356 ($\sim 40\%$) are also labelled in the figure. The remaining fraction of objects instead shows mixed properties in terms of final BH mass and/or lifetime in isolation (Δt , see Figure 2 in paperI).

The two ILS (5836 and 654) are shown by dot-dashed and dot-long dashed lines, respectively. Triangle-shaped (squared) data points indicate their growth during the Pop III star formation epoch (see Appendix A for further details). They start with comparable BH mass but follow a very different evolution. ILS-5836 grows much faster than the stellar mass (squares) until Pop II stars start to form in the host halo (dot-long dashed line) whereas ILS-654 evolves at an almost constant BH mass. In both systems the central BH experience mergers with other Pop III BHs formed in the same host galaxies (see Section 3.2 in paperI). These events cause the step-like increase in the BH mass along the two tracks (see Appendix A). The comparison with the average evolution of ILS, shown by the light blue squares, indicates that ILS-654 is more representative of the average ILS evolution. About 89% of systems are similar to ILS-654 while systems following an evolution (in terms of BH mass) similar to ILS-5836 are only $\sim 1\%$ of the population¹¹, as labelled in the figure.

A detailed description of evolutionary histories of the four prototypical systems is given in Appendix A.

We define the age of each system as the time it spends evolving in isolation from the formation of the BH seed (age = 0). The isolated evolution ends when the first (minor

or major) halo merger occurs. It is worth mentioning that although we follow systems in the “isolated” phase, this does not imply that the selected host halos evolve in isolation prior to seed BH formation. Thus, the initial conditions (e.g. gas mass and metallicity at age = 0) are different in different systems, even in those belonging to the same class. This reflects the different histories prior to BH seed formation and the host halo selection: ILS are initially hosted in star-forming mini halos, while IHS hosts are Ly α -cooling halos.

The four selected systems account for the large diversity in the properties of ILS and IHS populations. By looking at individual evolutionary histories (see Figure A1), we infer that BH growth is affected by (i) the environmental conditions at the epoch of BH seed formation (i.e. the properties of the host halo resulting from its earlier evolution) and, afterwards, (ii) by the host galaxy star formation and chemical enrichment histories. The final BH mass, at the end of the isolated evolution, is largely determined by these properties. Systems with similar (ILS-5836 and 654) or even equal (IHS-2538 and 13356) initial seed mass can follow very different evolutionary tracks reaching final BH masses that differ by ~ 2 orders of magnitude. Systems hosting BHs of different origins (IHS-2538 and ILS-5836) may instead end-up having similar properties (during certain stages of their evolution). These differences/similarities are reflected in the predicted SEDs.

4.2 Emission from BH seeds and their hosts

Following the procedure described in Section 3, we compute the SED of the selected IHS and ILS presented above at different times of their evolution (ages). Clearly, these correspond to different redshifts in the simulation. The results are shown in Fig. 3. The SED are represented by lighter colours at wavelengths where the emission will be completely absorbed by the intervening neutral hydrogen along the line of sight. These correspond to rest-frame wavelengths shortward of the Lyman limit at 912 Å, down to about ~ 100 Å (Madau 1995; Inoue et al. 2014, and references therein). In each panel, the yellow shaded and cyan dashed regions indicate the observed hard, [2-10] keV, and soft, [0.5-2] keV, X-ray bands. The gray arrow in the X-ray part of the spectrum identifies the range in the limiting fluxes of the ATHENA survey designed by Aird et al. (2013) for a ~ 1 deg² (lower end) and ~ 100 deg² (upper end) area¹². The gray triangles and squares report the NIRcam and MIRI photometric sensitivities on board of JWST¹³.

¹² This survey has been designed as a Wide Field Imager wedding cake strategy with single tiers of: 4×1 Ms, 20×300 ks, 75×100 ks and 259×30 ks. Reported flux limits are for a $3''$ PSF. A collecting area of $2m^2$ at 1 keV and an instrument field of view of $40' \times 40'$ have been assumed.

¹³ These are the photometric performance requirements of the instruments, namely, the point source faintest fluxes that can be obtained at a signal-to-noise ratio SNR = 10 in a 10ks integration (<https://jwst.stsci.edu/science-planning/proposal-planning-toolbox/sensitivity-overview>).

¹¹ Here we are considering all systems with $M_{\text{BH}} > 2 \times 10^4 M_\odot$ for this estimate

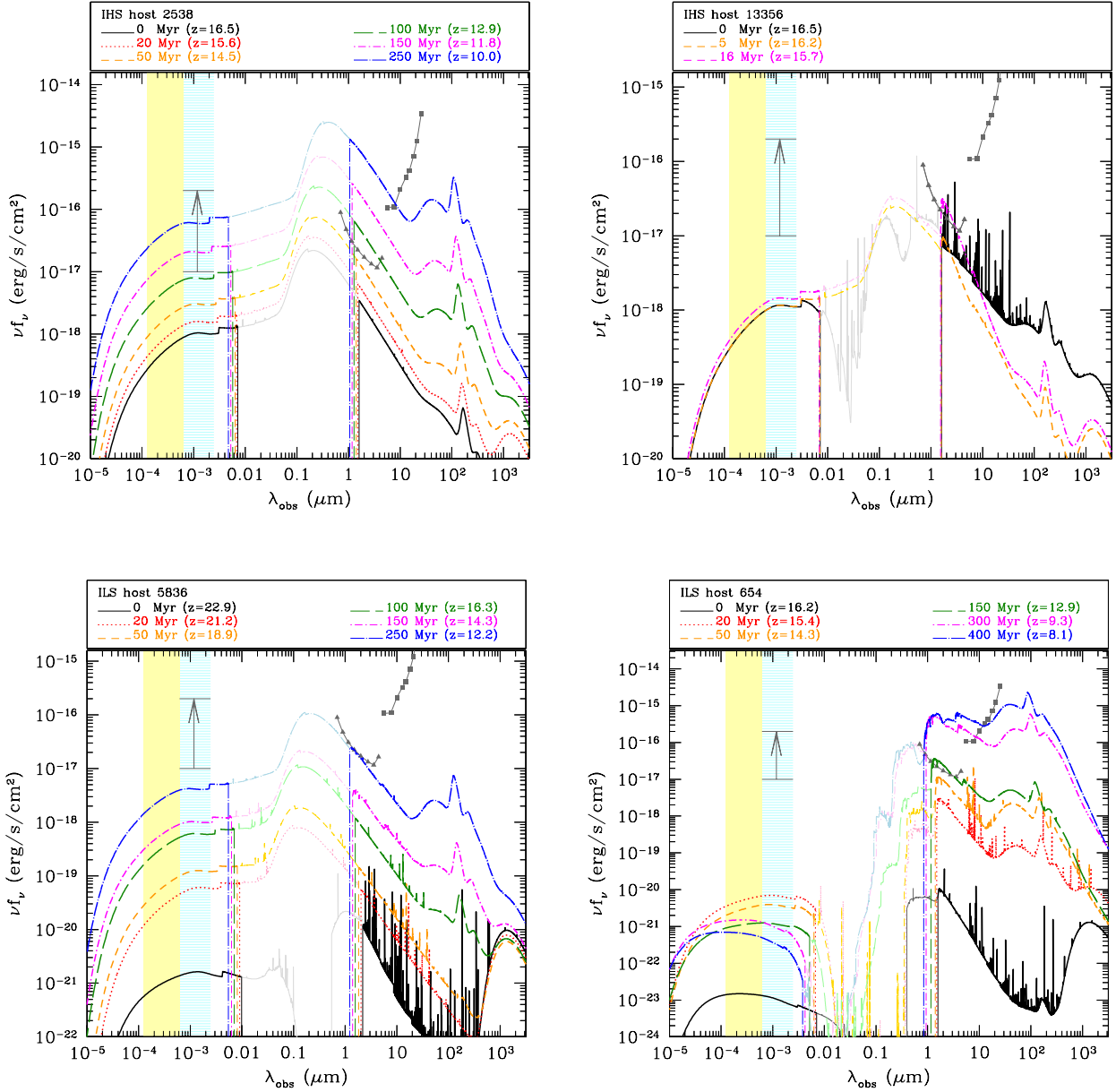


Figure 3. SED of IHS-2538 (top-left), IHS-13356 (top-right), ILS-5836 (bottom-left) and ILS-654 (bottom-right) as a function of the observed wavelength, λ_{obs} . In each panel, different lines corresponds to different ages of the system, as shown by the legends, where we also label the corresponding redshift in the simulation. The SED are shown by lighter colours at wavelengths where the emission will be completely absorbed by the intervening neutral hydrogen along the line-of-sight. The yellow shaded and cyan dashed regions indicate the observed hard and soft X-ray bands, respectively. The vertical arrow marks the flux limit of future surveys designed for the ATHENA mission by [Aird et al. \(2013\)](#). The gray triangles and squares are the photometric flux limits of the instruments NIRcam and MIRI on the JWST.

4.2.1 The most massive systems

We first analyze the time-dependent spectra of IHS-2538 (top-left) and ILS-5836 (bottom-left), which have been selected to be the most massive BHs among the IHS and ILS samples (see Fig. 2). At each epoch, the spectrum of IHS-2538 is dominated by the AGN continuum emission, resulting in an almost featureless SED (no prominent, luminous emission lines can be identified). Although strongly attenu-

ated by the intervening material, the most prominent feature in the rest-frame SED is the optical/UV emission from the BH accretion disc (the Big Blue Bump, BBB). The reprocessed AGN emission extends to $\lambda_{\text{obs}} \sim 10 \mu\text{m}$ ¹⁴. At longer

¹⁴ We do not include polycyclic aromatic hydrocarbon (PAHs) particles in the computation, which are expected to radiate in the [1 – 13] μm range.

wavelengths, the SED is dominated by dust thermal emission. At age ≥ 100 Myr, when the BH mass is $M_{\text{BH}} > 7 \times 10^5 M_{\odot}$ and the BH accretion rate (BHAR) is $\dot{M}_{\text{BH}} > 0.01 M_{\odot}/\text{yr}$ (see the top-left panel in Fig. A1), the rest-frame optical-UV emission is redshifted to the near IR (NIR) bands and is detectable by NIRcam. At almost the same time the emission in the X-ray bands becomes intense enough to exceed the lower flux limit in the ATHENA survey.

The duration of the isolated evolution of ILS-5836 is comparable to that of IHS-2538 (~ 225 Myr), but this system is located at a much higher redshift. It forms at $z \sim 22.9$ and evolves in isolation down to $z \sim 12$. At age = 0, when the first Pop III stars form, the emission from the accreting $\sim 100 M_{\odot}$ BH is comparable to that coming from the stellar component. As the system evolves in time, the emission properties appear to be a scaled-down version of IHS-2538 (see also the bottom left panel of Fig. A1). However, more prominent emission lines are present. This is a consequence of the larger gas column density in the host galaxy of ILS-5836, due to the less efficient BH feedback. At age = 250 Myr, although its flux is still below the JWST limit, the SED of ILS-5836 is potentially indistinguishable, in terms of shape and spectral features, from that of IHS-2538.

4.2.2 The least massive systems

Quite different spectra are predicted for IHS-13356 and ILS-654, which have been selected to host the two inefficiently-growing BHs among the IHS and ILS sample (see Fig. 2). The SEDs of IHS-13356 are shown in the top-right panel of Fig. 3 at age = 0, 5 and 16 Myr. At age = 0, the only emitting source is the newly planted BH. Its radiation travels through a large gas column density, as the gas mass is ~ 20 times higher than in IHS-2538 at the same epoch (as discussed in the previous section). Among the several emission lines, H and He recombination lines are present. Although the continuum level is below the NIRcam photometric capability, some of the lines are intense enough to be detected by NIRspec, despite the very high redshift of the source. As the gas mass drops, at age ≥ 5 Myr, the spectra are dominated by the continuum. At 16 Myr, the part of the spectrum (magenta dot-dashed line) entering in the NIRcam filters at $1 \mu\text{m} < \lambda_{\text{obs}} < 3 \mu\text{m}$ is dominated by the stellar component ($M_* \sim 10^5 M_{\odot}$) and it is just above the sensitivity limits. At this stage, IHS-13356 emission could be revealed by NIRcam (F200W and F277W filters) onboard of JWST. This low-mass, inefficiently accreting BH, is predicted to be too faint to be detected in the X-ray bands, even with ATHENA sensitivity.

Finally, the bottom right panel of Fig. 3 shows the SED of the starburst dominated ILS-654. Similarly to IHS-13356, this is a slowly accreting light BH seed whose mass never exceeds $\sim 10^3 M_{\odot}$, even after 400 Myr of evolution. The continuum emission is dominated by the stellar component with the low-mass AGN contributing to the X-ray part of the spectrum, but the emission remains several orders of magnitude fainter than any current (and future) instrument sensitivity. As the galaxy evolves (age > 100 Myr) a continuum-dominated spectrum emerges. Such an intense stellar emission may be easily revealed by the JWST.

4.2.3 Detectability

To summarize, systems like IHS-2538 or ILS-654 in the latest stages of their evolution (age ≥ 100 Myr) could be easily detected by the JWST instruments NIRcam (at $\lambda \geq 0.9 \mu\text{m}$) and MIRI (at least in the two higher-sensitivity photometric filters, F560W and F770W). The NIR and mid-IR (MIR) luminosities of these objects are $L_{\text{NIR}} \gtrsim 10^{42}$ erg/s and $L_{\text{MIR}} \gtrsim 10^{43}$ erg/s, respectively¹⁵. On the other hand, detecting objects like ILS-5836 would instead require deeper NIRcam campaigns. Interestingly, we find that the emission from a pure accreting heavy seed (no stars) enshrouded in a dense gas cloud, as in IHS-13356, may be revealed already at $z > 16$ by the spectrograph NIRspec, thanks to its prominent emission lines. The stellar-dominated radiation emerging afterwards (at $z \sim 15.7$) may be instead detected in the F200W and F277W NIRcam filters. Finally the ATHENA survey program envisioned in Aird et al. (2013) will reach flux limits which are exceeded only by accreting BH seeds similar to IHS-2538 at age > 100 Myr, when their soft X-ray luminosity becomes $L_{[0.5-2]\text{keV}} \geq 10^{42}$ erg/s.

We conclude that light and heavy seeds and their hosts can have very different emission properties. However, these appear to be more significantly affected by their individual evolutionary history rather than by their initial nature, i.e. whether they classify as a light or heavy BH seed. Yet, we recall that the two “antithetical” seed proto-types, IHS-2538 and ILS-654, show very different emission spectra: the first one being dominated by the central AGN and the second one being dominated by the stellar component of the host galaxy. While ILS-654 better represents the average evolution of light seeds, IHS-2538 represents $\sim 33\%$ of the IHS population. Still, systems like IHS-2538 are the most luminous among the IHS, thus, having the largest probability of being detected by JWST.

4.3 The mean IHS

As discussed above, the four selected prototypes represent extreme cases (the most and least efficiently growing IHS and ILS). In the ILS population, the results obtained for ILS-654 are also representative of the average population (see Figure 2). Thus, in order to make our predictions for IHS systems more general, we perform an additional analysis, by investigating the SEDs and observational properties of the “average” IHS population. To this aim we have constructed and processed AGN and stellar emission obtained by considering the average IHS evolution shown in Figure 2 (pink data points). The evolution of the mean IHS host has been weighted over the average lifetime in isolation, ~ 65 Myr (obtained from the distribution discussed in paper I)¹⁶.

The mean IHS is an AGN dominated system and its evolution is very similar (in both normalization and spectral features) to IHS-2538, although its final BH is less massive

¹⁵ These are the NIR and MIR band luminosities provided by Cloudy in the wavelength ranges $[1-5] \mu\text{m}$ and $[5-40] \mu\text{m}$, respectively.

¹⁶ For the mean IHS, age = 0, corresponds to the average formation redshift of heavy seeds, that is $z \sim 16.5$, the same redshift at which IHS-2538 forms. The final redshift, after ~ 65 Myr of isolated evolution, corresponds to $z \sim 13.9$.

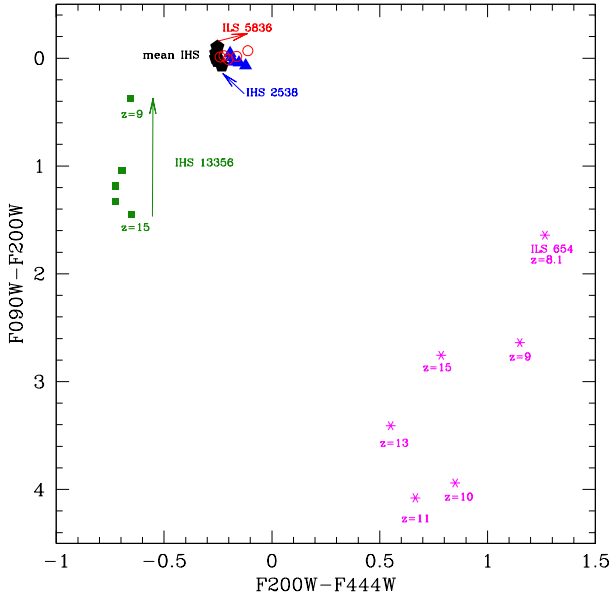


Figure 4. The color-color diagram for the selected proto-types at $z = 9, 10, 11, 13$ and 15 . IHS like 2538 and 13356 are shown by triangles and squares, respectively. Black pentagons are for the mean IHS case. ILS like 5836 and 654 are shown by circles and asterisks, respectively. For ILS-654 we also show the case $z = 8.1$, corresponding to the redshift at which the host reaches its maximum luminosity, at age = 400 Myr (see text). For other sources the arrows indicate the decreasing redshift direction.

Table 1. Bolometric luminosities of systems during the brightest stage of their evolution (see text for details).

name	age (Myr)	redshift	L_{bol} erg/s
IHS-2538	250	~ 10	$\sim 10^{45}$
IHS-13356	16	~ 16	$\sim 4 \times 10^{43}$
mean IHS	65	~ 13.9	$\sim 9.2 \times 10^{43}$
ILS-5836	225	~ 12	$\sim 5 \times 10^{43}$
ILS-654	405	~ 8.1	$\sim 3.5 \times 10^{44}$

($\sim 1.4 \times 10^6 M_{\odot}$ at 65 Myr). For this reason, we do not show the predicted time-dependent SED. In particular, the final stage of the mean IHS (i.e. at $age = 65$ Myr) its SED is comparable to that of IHS-2538 at $age = 100$ Myr (with the mean IHS, being potentially detectable by JWST). This is consistent with the fact that at these stages, when the BH mass is $\lesssim 10^6 M_{\odot}$, IHS-2538 and the mean IHS grows following similar evolutionary tracks.

4.4 Observational features of BH seeds and their hosts

To investigate the observability of growing BH seeds, we consider the systems presented above, compute their colours in the NIRcam filters and their X-ray luminosities.

To this aim, we first take the SED of each system during its brightest phase, which corresponds to different ages and redshifts (see Fig. 3). Bolometric luminosities of systems at

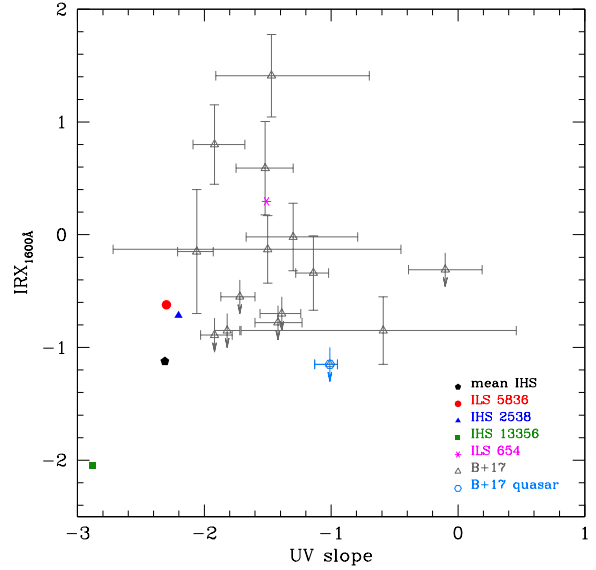


Figure 5. The IRX as a function of the UV continuum slope. Filled symbols represent IHS (2538 blue triangle, 13356 green square, mean IHS black pentagon) and ILS hosts (5836 red circle, 654 magenta asterisk). Empty data points with error bars are from Barisic et al. (2017), with the hexagon indicating a quasar candidate at $z = 5.3$.

the brightest stage are given in Table 1. During these phases, all the systems reach AB magnitudes $M_{\text{AB}} < 29$, above the JWST sensitivity limit for a 10 ks exposure in the $[0.7 - 4.4] \mu\text{m}$ spectral band¹⁷.

Then, we shift the above SED at $z = 9, 10, 11, 13$ and 15 , in order to compare the four systems at the same redshift¹⁸. This approach enables us to provide more general predictions, independently of the redshift at which the brightest stage is reached.

To compare with previous studies, we adopt the same colour-colour diagram proposed by Natarajan et al. (2017). The resulting F090W-F200W - F200W-F444W color diagram is shown in Fig. 4. The predicted colors reflect different galaxy types, with AGN-dominated systems (such as IHS-2538, the mean IHS and ILS-5836) being bluer than starbursts (ILS-654). The two classes are clearly distinguishable in the color-color plane, independently of their redshifts. Despite its lower AB magnitude¹⁹ we predict ILS-5836 to have very similar colors to IHS-2538. Hence, independently of their nature and of their redshifts, we find that efficiently growing BH seeds occupy a well defined region of the color-diagram.

In Fig. 5 we show the IRX–UV slope diagram for the

¹⁷ The four selected systems are F090W drop-outs, as the Lyman limit (912 \AA) is redshifted to longer wavelengths, with the exception of ILS-654 at $age \geq 300$ Myr (i.e. at $z \leq 9$).

¹⁸ At $z \geq 10$ these must be considered as upper limits as the Lyman-limit (912 \AA rest frame) falls in the F090W filter at these redshifts.

¹⁹ ILS-5836 reaches $M_{\text{AB}} \sim 29$ only at the end of its isolated evolution, at $z \sim 12$, and would be detectable with NIRcam at lower redshifts.

same systems and compare the results with the sample of $z \sim 5.5$ galaxies presented by Barisic et al. (2017). We compute the ratio between the rest frame IR and UV luminosities as $\text{IRX} = \log(L_{\text{IR}}/L_{1600\text{\AA}})$ and the UV continuum slopes, β , as a least-square linear fit in the $[1500 - 3000]\text{\AA}$ part of the spectra. Since the IRX is related to dust extinction, it is not surprising that the dustiest ($D_{\text{ISM}} \sim 5 \times 10^{-4}$, see Fig. A1) starburst prototype ILS-654 shows a high IRX, 0.29, and a spectral slope $\beta = -1.51$, consistent with some of the $z \sim 5.5$ observed galaxies (Mancini et al. 2016; Barisic et al. 2017). The IR luminosity (integrated from $8\ \mu\text{m}$ to $1000\ \mu\text{m}$) of this system is $L_{\text{IR}} \sim 10^{44}\text{ erg/s}$ ($\sim 85\%$ of the bolometric luminosity).

As expected, based on the similarity of their SED and colors, IHS-2538 and ILS-5836 have similar IRX and UV slopes. In these systems, the UV light from the accreting BHs is only mildly absorbed by the poorly enriched ISM of their host galaxies (see Fig. A1), resulting in a lower IRX, $\sim 0.6 - 0.7$, than in ILS-654. The mean IHS show a lower IRX with respect to IHS-2538 as a consequence of the lower associated dust-to-gas ratio (estimated by averaging over the dust-to-gas ratio of all the IHS systems). With respect to ILS-5836, the IRX of mean IHS has is lower because of its higher $L_{1600\text{\AA}}$.

Finally, the exceptionally blue slope ($\beta \sim -2.88$) and low IRX (~ -2.04) of IHS-13356 reflect the almost unattenuated, pure stellar emission dominating the SED at its maximum. The predicted β slope is consistent with the mean color of faint $z \sim 7$ galaxies measured by Bouwens et al. (2010).

The properties discussed above can be used to identify accreting BH seed candidates in future JWST surveys, distinguishing them from starbursts.

By combining the information obtained from color-color and IRX- β diagrams we suggest that the best candidates for future and deeper X-ray follow-up observational campaigns should be selected according to the following conditions:

- $-0.3 \lesssim F200W-F444W \lesssim 0$ and $F090W-F200W \gtrsim -0.2$
- UV continuum slopes $\beta < -2$ and $-1.5 < \text{IRX} < 0$.

One additional limitation to the observational identification of growing BH seeds is that the X-ray luminosities of faint BHs is hard to discriminate from the cumulative emission of high-mass X-ray binaries (HMXBs) in the host galaxies (e.g. Volonteri et al. 2017). In Fig. 6 we show the hard X-ray band luminosity, $L_{[2-10]\text{keV}} = L_{\text{AGN}} + L_{\text{HMXB}}$, as a function of the ratio between the AGN and HMXBs luminosities, $L_{\text{AGN}}/L_{\text{HMXB}}$, in the same spectral band. Following Volonteri et al. (2017), L_{HMXB} is computed using the empirical relation found by Lehmer et al. (2016), $\log(L_{\text{HMXB}}) = 39.82 + 0.63\log\dot{M}_* + 1.31\log(1+z)$, at the original redshift of the system in the simulation and at redshifts $z = 9, 10, 11, 13$ and 15^{20} .

We find that systems with properties similar to IHS-2538, the mean IHS and ILS-5836, have $L_{\text{AGN}}/L_{\text{HMXB}} > 100$. These would be easily identified as AGN. Although the SED of IHS-13356 is dominated by stellar emission (see Fig. 3) in the optical/UV (rest frame) part of the spectrum, a star

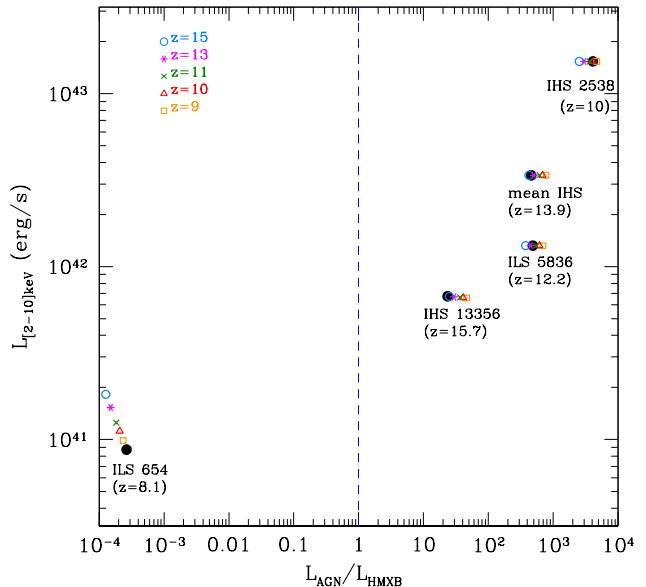


Figure 6. The relative contribution of accreting BHs and HMXBs to the luminosity at $[2 - 10]\text{keV}$ for the four prototypes in our sample: IHS-2538, IHS-13356, ILS-5836 and ILS-654, and the mean IHS. Black filled circles show the luminosity at the original redshift of the system while empty coloured symbols indicate the predictions at $z = 9$ (yellow squares), 10 (red triangles), 11 (green crosses), 13 (magenta asterisks) and 15 (azure circles). The blue vertical line depicts an equal contribution from AGN and HMXBs.

formation rate of $\dot{M}_* \sim 0.027 M_{\odot}/\text{yr}$ (see Fig. A1) corresponds to population of HMXBs that produce less than $\sim 5\%$ of the total luminosity at $[2 - 10]\text{keV}$ ($L_{\text{AGN}} \sim 6.5 \times 10^{41}\text{ erg/s}$ while $L_{\text{HMXB}} \sim 2.7 \times 10^{40}\text{ erg/s}$). On the other hand, the hard X-ray luminosity of IHS-654 would be dominated by HMXBs.

Our analysis shows that systems hosting rapidly growing BH seeds at their center (such as IHS-2538 and ILS-5836) can be easily discriminated from systems where the BH is almost inactive and/or the dominant emission comes from the host galaxy (such as ILS-654 and IHS-13356). They show bluer colors, intermediate IRX values and a high luminosity in the hard X-ray band, largely dominated by the accreting BH. On the other hand, the discrimination of the nature of the BH seed, whether it formed as a Pop III stellar remnant or as a DCBH, can be done only on the basis of statistical arguments.

5 COMPARISON WITH PREVIOUS WORKS

In their recent works, Pacucci et al. (2015) and Natarajan et al. (2017) suggest that JWST will be also able to discriminate among DCBH and Pop III remnant seeds by means of their spectral features. Similarly, we have explored the SED of growing DCBHs and Pop III remnant BHs, comparing the expected spectral features of the two different channels,

²⁰ The contribution of HMXBs has been computed only for the purpose of this comparison and it is not included in the SED models presented in Fig. 3.

in the same spirit of these earlier works but with some important differences.

The post-processing with Cloudy that we perform in our study is complementary to the one adopted by [Natarajan et al. \(2017\)](#). They consider an idealized set-up of a halo at a given redshift (with a given metallicity) while in our model the galaxy properties (e.g. the metallicity and dust-to-gas ratio) are derived from the cosmological evolution of the halos.

The adopted initial gas density profile in the model of [Pacucci et al. \(2015\)](#) results in SED with more prominent emission lines (mainly H and He recombination lines). In our simulation, similar gas densities and IR spectral features are found in halos 13356 and 5836, in the very early stages of their evolution, at ages $< 5 - 20$ Myr, when - however - AGN are faint $L_{\text{bol}} \leq 10^{43} - 10^{42}$, respectively.

On the other hand, the systems investigated by [Natarajan et al. \(2017\)](#) are the peculiar, transient OBGs ([Agarwal et al. 2013](#)). These are different from our IHS and ILS hosts, from the evolutionary point of view. In the scenario predicted by [Agarwal et al. \(2013\)](#), the newly formed DCBH host merge with a nearby star forming galaxy soon after the formation of the seed, in less than ~ 1 Myr. We find that, in a comparable time-scale, star formation in IHS hosts is enabled by the fast metal enrichment driven by gas-rich inflows from the IGM. Systems similar to IHS-2538, the most massive accreting heavy seed, at the end of their isolated evolution have properties consistent with an OBG, in terms of stellar and BH mass²¹.

If compared with previous works, our model shows how the emission depends on the environmental conditions in which the BH seeds form and grow. These conditions are determined by the assembly history of the $z \sim 6$ SMBH and its host galaxy²². Our predictions are for sources that would be seen in biased (over-dense) regions where $z > 6$ SMBH form and, thus, are somehow complementary with respect to other works.

In over-dense regions, the evolution of massive seeds (DCBHs) may be faster (more efficient) than in average volumes of the Universe (unbiased regions). In the latter case, the ISM evolution is strongly dominated by star formation, where SN feedback regulates the growth (and the feedback strength) of BH seeds in low-mass galaxies at early cosmic epochs (e.g. [Dubois et al. 2015](#); [Habouzit et al. 2017](#); [Bower et al. 2017](#); [Anglés-Alcázar et al. 2017](#); [Trebitsch et al. 2017](#)). In this scenario, growing BH seeds are similar to IHS-13356.

Conversely, in biased regions where $z > 6$ SMBH are expected to form, the early growth of some massive BH seeds ($\sim 33\%$ of the IHS population in our model) is self-regulated

by AGN feedback, as star formation (and thus SN feedback) is quenched as a consequence of the rapid build up of an intense UV background radiation (see Appendix A, paper I and V16 for details). The comparison with other studies, thus, points to a different evolution in biased (over dense) and unbiased (average volumes) regions. This is consistent with the discussion presented in paper I.

In deep blank-field surveys, we expect that sources predicted in our model, would be seen in over-dense regions that will later form $z \sim 6$ quasars (i.e. protoclusters, e.g. [Overzier 2016](#)).

We find that a color-color selection, similar to that proposed by [Natarajan et al. \(2017\)](#), would help in distinguishing AGN-dominated galaxies from starbursts. Although they have similar AB magnitudes ($M_{\text{AB}} \leq 26$ in the NIRcam bands), ILS-654-like starbursts are expected to be redder than OBGs and IHS-2538-like systems. On the other hand, despite the lower AB magnitude²³ rapidly growing ILS-5836 like systems have colors similar to IHS-2538 like ones, comparable to those expected for $z \sim 11$ OBGs. Thus, we find that a color-color selection is capable of uniquely identifying the nature of BH seeds only in a statistical sense. In fact, as we will show in the next section, rapidly growing BH seeds that originate from DCBHs have a higher probability of being detected, in agreement with previous findings ([Pacucci et al. 2015](#); [Natarajan et al. 2017](#)).

Another source of confusion in tracing the observational features of the first accreting BHs has been recently pointed out by [Volonteri et al. \(2017\)](#). The authors show that in high redshift galaxies, hosting < 1 Gyr old stellar populations, may be very difficult to distinguish stellar and AGN emission at rest frame UV/optical wavelengths. Moreover, the emission from low-mass AGN (powered by $10^5 - 10^6 M_{\odot}$ BHs), and from HMXB at $[2 - 10]$ keV would be difficult to disentangle at $z > 6$. The observational strategy we have suggested above would help in overcoming such a confusion problem.

6 SUMMARY AND CONCLUSIONS

In paper I we have investigated the physical properties of galaxies hosting light and heavy seeds in a cosmological context, following the formation and evolution of the first stars and BHs along the hierarchical assembly of a $z = 6.4$ quasar like SDSS J1148+5251. In this work we have used those properties to model the SEDs of both accreting BHs and their stellar counterparts, taking into account their redshift/time evolution as well as the effect of the interplay between, chemical, mechanical and radiative feedback on the host galaxies.

To this aim, we have selected four interesting objects from our sample of accreting BHs, two of which representative of the high-mass end of their population distributions, and two in the low-mass end, to emphasize differences and similarities between the two classes. We have extracted their evolutionary properties as long as their host galaxies evolve in isolation, only through mass exchanges with the external

²¹ For example, after living in isolation for 250 Myr, at $z = 10$, the IHS-2538 host galaxy merges with a normal star-forming galaxy (not hosting a BH in its center) with a stellar mass of $\sim 3 \times 10^7 M_{\odot}$ (before the merger). The properties of the galaxy formed by this merger are very similar to those expected for the OBGs discussed by [Agarwal et al. \(2013\)](#): the BH mass is $\sim 2 \times 10^7 M_{\odot}$ and the stellar mass is $\sim 4 \times 10^7 M_{\odot}$.

²² The assembly history determines the interplay between different physical processes (e.g. Pop III/Pop II star formation, onset of DCBH seeding conditions, BH growth, build up of UV background etc.) and their effects on the environment (via chemical, mechanical, and radiative feedback).

²³ ILS-5836 reaches $M_{\text{AB}} \sim 29$ only at the end of its isolated evolution, at $z \sim 12$, and would be detectable with NIRcam at lower redshifts.

medium (infall/outflows), with no mergers. Still, the evolution of these objects is influenced by (and influence) the evolution of the other galaxies polluting the external medium with metals and dust and permeating the virtual volume in which they reside with photo-dissociating and ionizing radiation.

For the selected objects we modeled the intrinsic emission coming from the accreting BHs and the stars. We then used these templates to predict the SED emerging from the host galaxy by processing the intrinsic emission using the software Cloudy. The information required to compute both the intrinsic and reprocessed emission, namely the Pop III remnant BH mass, BH accretion rate, and the properties of their host galaxies, such as the time evolving gas density, metallicity and dust-to-gas ratio were all consistently computed by the model GAMETE/QSO_{DUST}.

Our study attempts to answer two important questions: (i) *Can we detect the (growing) BH seed progenitors of the first SMBHs?* and if yes, (ii) *Can we identify the nature of BH seeds?*

To answer the first question, we confirm that future, high sensitivity facilities and missions, like JWST and ATHENA will be able to detect the most luminous ($L_{\text{NIR}} \geq 10^{42}$ erg/s; $L_{\text{MIR}} \geq 10^{43}$ erg/s; $L_{[0.5-2]\text{keV}} \geq 10^{42}$ erg s⁻¹) progenitors of the first SMBHs.

Regarding the second question, searches for growing BH seeds must be extended out to $z > 10$, when the probability of observing them in isolation is expected to be higher (see paperI). It is also interesting to note that at $z \lesssim 15(17)$, for IHS (ILS), at least half of the BHs are still in isolated systems. At lower redshift, BH seeds and their host galaxies rapidly loose memory of their initial conditions (see paperI for details).

Among $z > 6$ SMBH progenitors, rapidly growing BH seeds at $z > 10$ that are luminous enough to be detectable with JWST, in the field of a quasar, are only 2% of the total BH seed population. This percentage corresponds to an average number of $\sim 4^{+3}_{-2}$ (at a 1σ confidence level, assuming Poissonian statistics) progenitors for each $z \sim 6$ SMBH. Their average redshift distribution is shown in Figure 7, where we also discriminate IHS (red histogram) and ILS (blue histogram). Hence, a JWST detected BH progenitor at $z > 10$ has a larger probability to originate from a DCBH than from a Pop III remnant. Our conclusion is that it will be difficult to discriminate the nature of $z \sim 6$ SMBHs seeds on the basis of their observational features as Pop III BHs and DCBHs look very similar when they are above JWST or ATHENA sensitivity limits. However, if detected, these systems are more likely powered by a growing DCBH.

Interestingly, with a 10 ks NIRcam observation, sources like IHS-13356 can be detected with a SNR= 10 in the F200W and F277W filters, already at $z \sim 15.7$. In addition, we foresee that blind search programs conducted with the spectrograph NIRspec would allow to reveal these kind of systems even at earlier epochs ($z > 16$), thanks to the strong emission lines emerging in the spectra.

We believe that a multi-wavelength approach will be fundamental in searching the first SMBH progenitors. While JWST will be able to characterize their host galaxies, the high ATHENA flux sensitivity ($\sim 10^{-17}$ erg/s/cm² at [0.5 – 2] keV, [Nandra et al. 2013](#)) will allow to uncover the signatures of accreting BHs. A IR color-color plus IRX- β selection of

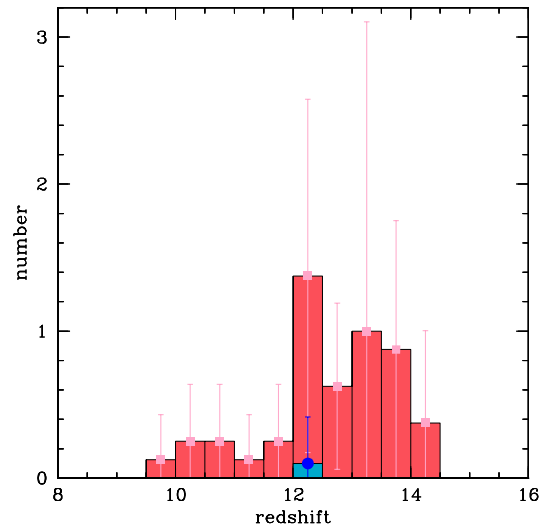


Figure 7. The redshift distribution of detectable IHS (red) and ILS (blue). Histograms and data points show the average number over 10 different realizations with error bars indicating the 1σ dispersion. In each redshift bin, we show the number of systems with $L_{\text{bol}} \geq 4 \times 10^{43}$ erg/s ($M_{\text{BH}} \geq 3.5 \times 10^5 M_{\odot}$).

high redshift JWST sources could help in successfully identify possible SMBH progenitors candidates in future X-ray surveys, also providing a unique tool for preparing follow-up observations.

Finally, we stress that the above conclusions apply to a scenario where SMBHs at $z \sim 6$ originate from the Eddington-limited growth of Pop III BHs and DCBHs. If Pop III stellar remnants are able to sustain short and intermittent phases of super-Eddington accretion ([Pezzulli et al. 2016](#)), their occurrence and observational properties may be different.

ACKNOWLEDGMENTS

The research leading to these results has received funding from the European Research Council under the European Union’s Seventh Framework Programme (FP/2007-2013) / ERC Grant Agreement n. 306476. LZ acknowledges financial support under ASI/INAF contract 1/037/12/0. We thank Angela Bongiorno, Fabrizio Fiore, Emanuele Giallongo, Michele Ginolfi, Andrea Grazian, Tilman Hartwig, Elisabeta Lusso and Laura Pentericci for fruitful discussions.

REFERENCES

- Agarwal B., Davis A. J., Khochfar S., Natarajan P., Dunlop J. S., 2013, *MNRAS*, **432**, 3438
- Agarwal B., Dalla Vecchia C., Johnson J. L., Khochfar S., Paardekooper J.-P., 2014, *MNRAS*, **443**, 648
- Agarwal B., Johnson J. L., Zackrisson E., Labbe I., van den Bosch F. C., Natarajan P., Khochfar S., 2016, *MNRAS*, **460**, 4003
- Agarwal B., Johnson J. L., Khochfar S., Pellegrini E., Rydberg C.-E., Klessen R. S., Oesch P., 2017, preprint, ([arXiv: 1702. 00407](#))

- Aird J., Comastri A., Brusa M., Cappelluti N., Moretti A., Vanzella e. a., 2013, preprint, ([arXiv:1306.2325](#))
- Anglés-Alcázar D., Faucher-Giguère C.-A., Quataert E., Hopkins P. F., Feldmann R., Torrey P., Wetzel A., Kereš D., 2017, *MNRAS*, **472**, L109
- Barisic I., et al., 2017, *ApJ*, **845**, 41
- Begelman M. C., Volonteri M., Rees M. J., 2006, *MNRAS*, **370**, 289
- Bouwens R. J., et al., 2010, *ApJ*, **708**, L69
- Bower R. G., Schaye J., Frenk C. S., Theuns T., Schaller M., Crain R. A., McAlpine S., 2017, *MNRAS*, **465**, 32
- Bowler R. A. A., McLure R. J., Dunlop J. S., McLeod D. J., Stanway E. R., Eldridge J. J., Jarvis M. J., 2016, arXiv.org, p. arXiv:1609.00727
- Brightman M., Silverman J. D., Mainieri V., Ueda Y., Schramm M., et al. M., 2013, *MNRAS*, **433**, 2485
- Bromm V., Loeb A., 2003, *ApJ*, **596**, 34
- Burlon D., Ajello M., Greiner J., Comastri A., Merloni A., Gehrels N., 2011, *ApJ*, **728**, 58
- Cappelluti N., Comastri A., Fontana A., Zamorani G., Amorin R., Castellano M., Merlin E. e. a., 2016, *ApJ*, **823**, 95
- Chon S., Hirano S., Hosokawa T., Yoshida N., 2016, *ApJ*, **832**, 134
- Cicone C., et al., 2015, *A&A*, **574**, A14
- Cowie L. L., Songaila A., 1986, *ARA&A*, **24**, 499
- Davies R. I., et al., 2006, *ApJ*, **646**, 754
- Davies R. I., Müller Sánchez F., Genzel R., Tacconi L. J., Hicks E. K. S., Friedrich S., Sternberg A., 2007, *ApJ*, **671**, 1388
- Di Matteo T., Springel V., Hernquist L., 2005, *Nature*, **433**, 604
- Dijkstra M., Ferrara A., Mesinger A., 2014, *MNRAS*, **442**, 2036
- Dijkstra M., Gronke M., Sobral D., 2016, *ApJ*, **823**, 74
- Dubois Y., Volonteri M., Silk J., Devriendt J., Slyz A., Teyssier R., 2015, *MNRAS*, **452**, 1502
- Ferland G. J., et al., 2013, *Rev. Mex. Astron. Astrofis.*, **49**, 137
- Ferrara A., Salvadori S., Yue B., Schleicher D., 2014, *MNRAS*, **443**, 2410
- Fioc M., Rocca-Volmerange B., 1997, *A&A*, **326**, 950
- Fioc M., Rocca-Volmerange B., 1999, *ArXiv Astrophysics e-prints*,
- Gallerani S., Fan X., Maiolino R., Pacucci F., 2017, *Publ. Astron. Soc. Australia*, **34**, e022
- Georgakakis A., et al., 2015, *MNRAS*, **453**, 1946
- Giallongo E., Grazian A., Fiore F., Fontana A., Pentericci L., Vanzella E. e. a., 2015, *A&A*, **578**, A83
- Habouzit M., et al., 2016, *MNRAS*, **456**, 1901
- Habouzit M., Volonteri M., Dubois Y., 2017, *MNRAS*, **468**, 3935
- Haiman Z., 2004, *ApJ*, **613**, 36
- Hartwig T., Glover S. C. O., Klessen R. S., Latif M. A., Volonteri M., 2015, *MNRAS*, **452**, 1233
- Heger A., Fryer C. L., Woosley S. E., Langer N., Hartmann D. H., 2003, *ApJ*, **591**, 288
- Hicks E. K. S., Davies R. I., Malkan M. A., Genzel R., Tacconi L. J., Müller Sánchez F., Sternberg A., 2009, *ApJ*, **696**, 448
- Hirano S., Hosokawa T., Yoshida N., Omukai K., Yorke H. W., 2015, *MNRAS*, **448**, 568
- Hosokawa T., Omukai K., Yorke H. W., 2012, *ApJ*, **756**, 93
- Hosokawa T., Yorke H. W., Inayoshi K., Omukai K., Yoshida N., 2013, *ApJ*, **778**, 178
- Inayoshi K., Haiman Z., 2014, *MNRAS*, **445**, 1549
- Inayoshi K., Omukai K., 2012, *MNRAS*, **422**, 2539
- Inayoshi K., Omukai K., Tasker E., 2014, *MNRAS*, **445**, L109
- Inayoshi K., Visbal E., Kashiyama K., 2015, *MNRAS*, **453**, 1692
- Inoue A. K., Shimizu I., Iwata I., Tanaka M., 2014, *MNRAS*, **442**, 1805
- Johnson J. L., Haardt F., 2016, *Publ. Astron. Soc. Australia*, **33**, e007
- Larson R. B., 1998, *MNRAS*, **301**, 569
- Latif M. A., Ferrara A., 2016, *Publ. Astron. Soc. Australia*, **33**, e051
- Latif M. A., Schleicher D. R. G., Schmidt W., Niemeyer J. C., 2013, *MNRAS*, **436**, 2989
- Lehmer B. D., Basu-Zych A. R., Mineo S., Brandt W. N., Eufrazio R. T., Fragos e. a., 2016, *ApJ*, **825**, 7
- Lodato G., Natarajan P., 2006, *MNRAS*, **371**, 1813
- Lodato G., Natarajan P., 2007, *MNRAS*, **377**, L64
- Luo B., et al., 2017, *ApJS*, **228**, 2
- Madau P., 1995, *ApJ*, **441**, 18
- Madau P., Rees M. J., 2001, *ApJ*, **551**, L27
- Madau P., Rees M. J., Volonteri M., Haardt F., Oh S. P., 2004, *ApJ*, **604**, 484
- Magdziarz P., Zdziarski A. A., 1995, *MNRAS*, **273**, 837
- Maiolino R., et al., 2012, *MNRAS*, **425**, L66
- Mancini M., Schneider R., Graziani L., Valiante R., Dayal P., Maio U., Ciardi B., 2016, *MNRAS*, **462**, 3130
- Mather J. C., Fixsen D. J., Shafer R. A., Mosier C., Wilkinson D. T., 1999, *ApJ*, **512**, 511
- Mathis J. S., Rimpl W., Nordsieck K. H., 1977, *ApJ*, **217**, 425
- Matthee J., Sobral D., Santos S., Röttgering H., Darvish B., Mobasher B., 2015, *MNRAS*, **451**, 400
- Mullman K. L., Lawler J. E., Zsargó J., Federman S. R., 1998, *ApJ*, **500**, 1064
- Nandra K., et al., 2013, preprint, ([arXiv:1306.2307](#))
- Natarajan P., 2011, preprint, ([arXiv:1105.4902](#))
- Natarajan P., Pacucci F., Ferrara A., Agarwal B., Ricarte A., Zackrisson E., Cappelluti N., 2017, *ApJ*, **838**, 117
- Overzier R. A., 2016, *A&ARv*, **24**, 14
- Pacucci F., Ferrara A., Volonteri M., Dubus G., 2015, *MNRAS*, **454**, 3771
- Pacucci F., Ferrara A., Grazian A., Fiore F., Giallongo E., Puccetti S., 2016, *MNRAS*, **459**, 1432
- Pacucci F., Pallottini A., Ferrara A., Gallerani S., 2017, *MNRAS*, **468**, L77
- Pallottini A., et al., 2015, *MNRAS*, **453**, 2465
- Peebles P. J. E., 1971, *Physical cosmology*
- Petri A., Ferrara A., Salvaterra R., 2012, *MNRAS*, **422**, 1690
- Pezzulli E., Valiante R., Schneider R., 2016, *MNRAS*, **458**, 3047
- Pezzulli E., Valiante R., Orofino M. C., Schneider R., Gallerani S., Sbarrato T., 2017, *MNRAS*, **466**, 2131
- Reines A. E., Comastri A., 2016, *Publ. Astron. Soc. Australia*, **33**, e054
- Salvadori S., Schneider R., Ferrara A., 2007, *MNRAS*, **381**, 647
- Salvadori S., Ferrara A., Schneider R., 2008, *MNRAS*, **386**, 348
- Sani E., Marconi A., Hunt L. K., Risaliti G., 2011, *MNRAS*, **413**, 1479
- Sani E., et al., 2012, *MNRAS*, **424**, 1963
- Savage B. D., Sembach K. R., 1996, *ARA&A*, **34**, 279
- Sazonov S. Y., Ostriker J. P., Sunyaev R. A., 2004, *MNRAS*, **347**, 144
- Schaerer D., 2002, *A&A*, **382**, 28
- Schneider R., Ferrara A., Natarajan P., Omukai K., 2002, *ApJ*, **571**, 30
- Schneider R., Ferrara A., Salvaterra R., Omukai K., Bromm V., 2003, *Nature*, **422**, 869
- Schneider R., Omukai K., Bianchi S., Valiante R., 2012, *MNRAS*, **419**, 1566
- Shakura N. I., Sunyaev R. A., 1973, *A&A*, **24**, 337
- Smidt J., Wiggins B. K., Johnson J. L., 2016, *ApJ*, **829**, L6
- Smith A., Bromm V., Loeb A., 2016, *MNRAS*, **460**, 3143
- Snow T. P., Destree J. D., Jensen A. G., 2007, *ApJ*, **655**, 285
- Sobral D., Matthee J., Darvish B., Schaefer D., Mobasher B., Röttgering H. J. A., Santos S., Hemmati S., 2015, *ApJ*, **808**, 139
- Sugimura K., Coppola C. M., Omukai K., Galli D., Palla F., 2015, arXiv:1509.04562,
- Tanaka T., Haiman Z., 2009, *ApJ*, **696**, 1798

- Trebitsch M., Volonteri M., Dubois Y., Madau P., 2017, preprint, (arXiv: 1712.05804)
- Treister E., Schawinski K., Volonteri M., Natarajan P., 2013, *ApJ*, **778**, 130
- Valiante R., Schneider R., Salvadori S., Bianchi S., 2011, *MNRAS*, **416**, 1916
- Valiante R., Schneider R., Maiolino R., Salvadori S., Bianchi S., 2012, *MNRAS*, **427**, L60
- Valiante R., Schneider R., Salvadori S., Gallerani S., 2014, *MNRAS*, **444**, 2442
- Valiante R., Schneider R., Volonteri M., Omukai K., 2016, *MNRAS*
- Valiante R., Schneider R., Graziani L., Zappacosta L., 2017a, preprint, (arXiv: 1711.11033)
- Valiante R., Agarwal B., Habouzit M., Pezzulli E., 2017b, *Publ. Astron. Soc. Australia*, **34**, e031
- Visbal E., Haiman Z., Bryan G. L., 2016, *MNRAS*, **460**, L59
- Vito F., et al., 2016, *MNRAS*, **463**, 348
- Volonteri M., 2010, *ARA&A*, **18**, 279
- Volonteri M., Rees M. J., 2005, *ApJ*, **633**, 624
- Volonteri M., Rees M. J., 2006, *ApJ*, **650**, 669
- Volonteri M., Haardt F., Madau P., 2003, *ApJ*, **582**, 559
- Volonteri M., Lodato G., Natarajan P., 2008, *MNRAS*, **383**, 1079
- Volonteri M., Silk J., Dubus G., 2015, *ApJ*, **804**, 148
- Volonteri M., Reines A., Atek H., Stark D. P., Trebitsch M., 2017, preprint, (arXiv: 1704.00753)
- Wada K., Papadopoulos P. P., Spaans M., 2009, *ApJ*, **702**, 63
- Weigel A. K., Schawinski K., Treister E., Urry C. M., Koss M., Trakhtenbrot B., 2015, *MNRAS*, **448**, 3167
- Wilkinson D. T., 1987, in Ulmer M. P., ed., 13th Texas Symposium on Relativistic Astrophysics. pp 209–218
- Willott C. J., 2011, *ApJ*, **742**, L8
- Yoshida N., Omukai K., Hernquist L., 2008, *Science*, **321**, 669
- Yue B., Ferrara A., Salvaterra R., Xu Y., Chen X., 2013, *MNRAS*, **433**, 1556
- Yue B., Ferrara A., Salvaterra R., Xu Y., Chen X., 2014, *MNRAS*, **440**, 1263
- de Bressan M., Schneider R., Valiante R., Salvadori S., 2014, *MNRAS*, **445**, 3039
- de Bressan M., Salvadori S., Schneider R., Valiante R., Omukai K., 2017, *MNRAS*, **465**, 926

APPENDIX A: PROPERTIES OF INDIVIDUAL SYSTEMS

In this appendix we provide a detailed description of the evolutionary histories of the four prototypical systems.

We present the time dependent properties of systems IHS-2538, IHS-13356, ILS-5836 and ILS-654 in Fig. A1. For each system, in the upper panel we show the DM (dotted line), gas (dashed), stellar (dot-dashed) and BH (solid) masses. In the upper horizontal axis we also label the redshifts in the simulation that correspond to the different ages. The star formation and BH accretion rates are shown in the middle panel with dot-dashed and solid lines respectively. Finally, the lower panel reports the gas-phase metals (Z_{ISM} , dotted-dashed line) and dust-to-gas mass ratio (D_{ISM} , dashed line) in the ISM (in absolute units). For comparison, we also show the critical metallicity, $Z_{\text{cr}} \sim 10^{-4} Z_{\odot}$ (dotted horizontal line), which marks the transition from Pop III to Pop II star formation.

IHS-2538: this is one of the most massive and longest-living isolated heavy seeds. By construction, the initial BH has a mass of $10^5 M_{\odot}$ and forms in a Ly α cooling halo ($M_{\text{h}} \sim 5 \times 10^7 M_{\odot}$) at redshift $z = 16.5$. Such a DM

halo is the descendant of two sterile mini-halos. For its entire history, the heavy seed grows close to or at the Eddington rate. Efficient BH feeding and feedback enable the galaxy to sustain only a very low star formation rate ($< 3 \times 10^{-3} M_{\odot}/\text{yr}$). As a result, the BH always grows faster than the stellar component, and the SED properties are expected to be dominated by the AGN emission.

IHS-13356: this is one of the shortest-living and smallest isolated heavy seeds. Differences in the histories of IHS-13356 progenitors, relative to IHS-2538, lead to different initial gas masses at age = 0. The reason for this behaviour can be understood as follows: newly virialized halos gradually accrete their gas mass following an exponentially decaying infall rate until they merge with another halo (i.e. they do not instantaneously acquire the universal baryon fraction $\Omega_{\text{b}}/\Omega_{\text{M}}$; see eq. 3 and further details in Salvadori et al. 2008). IHS-13356 is hosted in a Ly α cooling halo formed by the merger of two sterile mini-halos at $z = 16.5$. These ancestors virialize at $z \sim 17$ and accrete a gas mass which corresponds to $\sim 40\%$ of $\Omega_{\text{b}}/\Omega_{\text{M}}$ prior to their coalescence. Conversely, IHS-2538 is hosted in a Ly α cooling halo that has formed soon after its progenitor mini-halos virialize, so that they accrete only $\sim 1\%$ of $\Omega_{\text{b}}/\Omega_{\text{M}}$ by the time they coalesce. When IHS-13356 forms, the coalescence of its gas-rich ancestors triggers an efficient starburst of $\sim 2 \times 10^{-2} M_{\odot}/\text{yr}$. The gas mass suddenly drops from $\sim 2 \times 10^6 M_{\odot}$ to $\sim 10^5 M_{\odot}$ within the first 0.5 Myr, corresponding to the time step of the simulation at that redshift. Thereafter, IHS-13356 evolves in gas starvation, with star formation, BH accretion and the associated mechanical feedback depleting almost all the gas mass that the halo is accreting from the intergalactic medium. At the end of the brief (16 Myr) isolated evolution, the nuclear BH mass has increased by $\sim 50\%$ and the stellar mass is a factor ~ 2.5 larger. The emission properties of this system are dominated by the AGN during the first 5 Myr of the evolution (when $M_{\star} < 10^5 M_{\odot}$), and by the emission of the host galaxy thereafter.

ILS-5836: this is one of the most massive isolated light seeds. Its host halo is one of the first star forming mini-halos ($M_{\text{h}} \sim 4 \times 10^6 M_{\odot}$) at redshift $z \sim 23$. Due to its pristine composition, a first burst of Pop III stars ($10^{-3} M_{\odot}/\text{yr}$) leads to the formation of one massive BH remnant with $M_{\text{BH}} \sim 70 M_{\odot}$. Pop III star formation continues for about 100 Myrs, down to redshift $z \sim 16.2$, but with a ~ 50 Myr suppression due to the effect of the LW flux at which the mini-halo is exposed. Due to their short evolutionary timescales, massive Pop III stars are assumed to evolve in one simulation timestep (instantaneous recycling approximation). Hence $M_{\star} = 0$ when the $\dot{M}_{\star} = 0$. When the DM halo has become a Ly α cooling halo, Pop III star formation turns on again and continues until metal enrichment triggers the transition to Pop II star formation, in the last ~ 125 Myr of evolution. During the Pop III regime, the nuclear BH grows by gas accretion and mergers with other remnant BHs forming in subsequent bursts, reaching a mass of $\sim 10^4 M_{\odot}$ in ~ 70 Myr. The gas accretion rate triggered during the non-star forming phase leads to a BH dominance scenario even in the subsequent Pop II star formation regime: in ILS-5836, the BH mass continues to grow faster than its stellar counterpart. At $z \sim 12.2$, the BH mass has

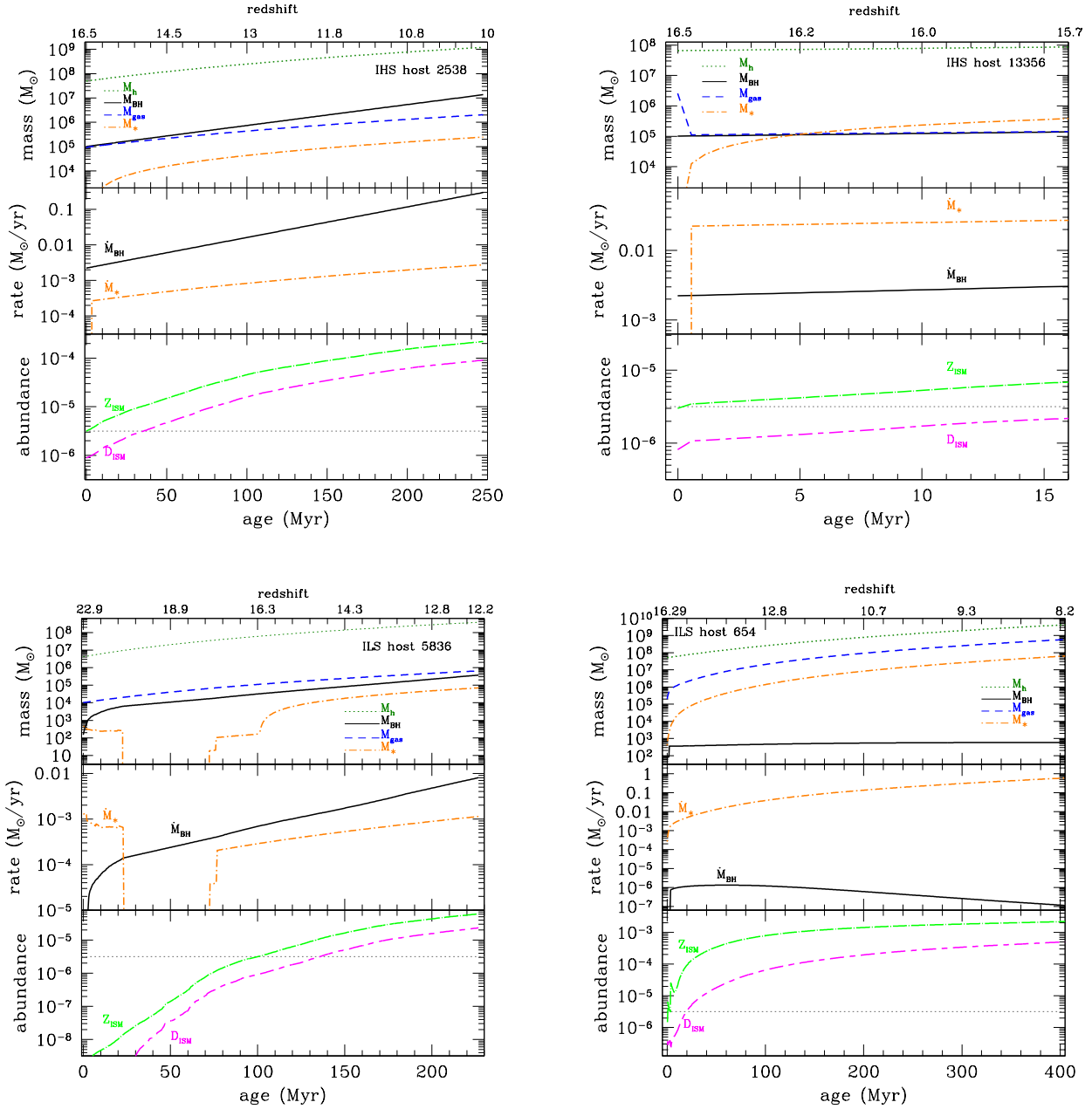


Figure A1. Time dependent properties of IHS-2538 (top left), IHS-13356 (top right), ILS-5836 (bottom left) and ILS-654 (bottom right). For each system, the upper panel shows the DM halo (dotted line), gas (dashed line), stellar (dot-dashed line) and BH (solid line) masses. The middle panel shows the star formation (dot-dashed) and black hole accretion (solid) rates. The lower panel shows the metallicity (dotted-dashed line) and dust-to-gas mass ratio (dashed line) of the ISM, in absolute units. The horizontal dotted line indicates the critical metallicity for the Pop III/Pop II star transition.

grown to $4 \times 10^5 M_{\odot}$. This evolution is reflected in the SED, that is a sort of scaled-down version of the SED of IHS-2538.

ILS-654: this is one of the least massive but longest-living isolated light seeds. Inefficient BH accretion [$\dot{M}_{\text{BH}} \sim (10^{-7} - 10^{-6}) M_{\odot}/\text{yr}$] leads to a final mass of only $800 M_{\odot}$ in more than 400 Myr of evolution. Although they have similar initial BH masses and accretion rates, $\sim 10^{-6} M_{\odot}/\text{yr}$ at age = 0, BH-growth in ILS-5836 at early times is mainly driven by

mergers with other Pop III BH remnants during the prolonged Pop III star formation in this halo. As a consequence of the low BH growth of ILS-654, the available gas mass can efficiently fuel star formation, yielding to a star formation rate $> 0.01 M_{\odot}/\text{yr}$ already at age > 30 Myr. The evolution of ILS-654 is indeed consistent with that of a normal star-forming galaxy, and the system becomes the most metal-rich of the four selected objects. In addition, in the absence of efficient BH accretion and feedback more infalling gas is re-

tained and the higher metallicity, dust-to-gas ratio and gas density are reflected in the predicted SED.

This paper has been typeset from a $\text{\TeX}/\text{\LaTeX}$ file prepared by the author.